Journal of Stress Analysis
Vol. 5, No. 1, Spring − Summer 2020, 31-47

Bu-Ali Sina University

ORIGINAL RESEARCH PAPER

Magneto-piezo-mechanical Stresses Analysis of a Porous FGPM Rotating Non-uniform Thickness Disc with Variable Angular Velocity

M. Saadatfar*, **M.H. Zarandi**

Mechanical Engineering Department, University of Qom, Qom, Iran.

Article info

Article history:
Received 24 February 2020
Received in revised form
05 June 2020
Accepted 20 May 2020

Keywords:
Rotating disc
Variable thickness
Variable angular speed
Porosity
FGPM
Magnetic field

Abstract

The mechanical behavior of a fluid-saturated Functionally Graded Porous Piezoelectric Material (FGPPM) rotating disc with variable angular velocity and thickness placed in a constant magnetic field was investigated. Due to variable angular velocity, the disc was subjected to Lorentz force in two directions: radial and circumferential. It was assumed the disc is power-law functionally graded in the radial direction. The disc is uniformly porous and its thickness varies as a function of radius. First, three coupled governing partial differential equations were converted to ordinary differential equations using the separation of variable technique. Then, equations were solved using Runge-Kutta and shooting methods for the case of fixed-free boundary condition. The effect of variable angular velocity, thickness profile, inhomogeneity index, porosity and magnetic field was investigated. The results demonstrate that considering angular acceleration for the disc has a considerable effect on the Lorentz force resulted by the magnetic field. Besides, the angular velocity constant has a significant effect on the stresses and displacements in the presence of the magnetic field.

Nomenclature

English parameters			
c_{ij}	Elastic constants	d_{11}	Electromagnetic constant
D_i	Components of electric displacement	e	Volumetric strain
e_{ij}	Piezoelectric constants	$\vec{E}$	Induced electric field
E_i	Components of electric field	f_i	Components of body forces
$\vec{h}$	Induced magnetic field	h_0	Outer thickness
h_i	Inner thickness	$\vec{H}$	Magnetic field vector
$\vec{J}$	Electric current density vector	K	Drained bulk modulus
K_u	Undrained bulk modulus	K_f	Bulk modulus of the fluid
p	Pore fluid pressure	r_i	Inner radius
r_o	Outer radius	S	Thickness index
u_i	Displacement components		

*Corresponding author: M. Saadatfar (Assistant Professor)
E-mail address: m.saadatfar@gmail.com
http://dx.doi.org/10.22084/jrstan.2020.21129.1133
ISSN: 2588-2597

Greek parameters			
ω_0	Initial angular velocity	α	Biot's coefficient of effective stress
β	Inhomogeneity index	Δr	Step size in Runge-Kutta method
ε_e	Electric permeability	ε_i	Components of strain
ϵ_i	Dielectric constants	λ	Angular velocity constant
μ	Magnetic permeability	$\mathcal{M}$	Biot's modulus
ξ	Variation of the fluid content	ρ	Density
σ_i	Components of stress	τ_{ij}	Components of shear
φ	Porosity	ϕ	Electric potential
$\Phi_i(\Phi_o)$	Electric potential at the inner (outer) radius	ω	Angular velocity function
$\dot{\omega}$	Angular acceleration		

1. Introduction

Nowadays, smart structures have attracted much focus in the area of research and industrial usage [1-3]. Functionally graded smart materials such as Functionally Graded Piezoelectric Material (FGPM) and Functionally Graded Magneto-Electro-Elastic (FGMEE), which are used as sensors or actuators, have several applications in engineering areas [4]. Due to having functionally graded properties, this sensors and actuators exhibit better performance than homogeneous ones [5, 6]. Furthermore, rotating discs are increasingly used in many mechanical structures such as compressors, turbo generators, flywheels, gas turbine rotors, automotive braking systems, ship propellers and computer disc drives [7-10]. Therefore, the prediction of the behavior of discs made of smart materials under various loads and environmental conditions is an interesting study field for engineering researchers. Accordingly, some researchers tried to analyze the different behavior of FGPM rotating discs. Dai et al. [11] investigated the elastic behavior of a rotating FGPM disc under hygrothermal loads. Loghman et al. [12] studied FGPM rotating disc and considered creep behavior. Ghorbanpour et al. [13] investigated the effects of thermal and magnetic loads on the behavior of FGPM rotating discs. Saadatfar [14] analyzed the time-dependent creep response of Magneto-Electro-Elastic (MEE) rotating disc in thermal and humid environmental condition.

Since there are many applications for rotating discs with variable thickness in industrial usage, many articles were presented to study different behaviors of them. Bayat et al. [15] researched into variable thickness FGM rotating discs under different boundary conditions. Bayat et al. [16, 17] studied thermal stresses in rotating FGM with variable thickness. Zenkour and Mashat [18] solved the problem of variable thickness rotating discs analytically and numerically. Zafarmand and Hassani [19] studied two-dimensional FGM discs with variable thickness. Thawait et al. [20] worked on concave thickness FGM rotating disc. Semi-analytical solution for stress distribution in exponentially graded rotating discs with arbitrary thickness variations was presented by Allam et al. [21]. Vullo and Vivio [22] presented an analytical method for analysis of thermal stresses and displacements in variable thickness rotating discs having density variation radially. Deepak et al. [23] investigated creep behavior in FGM rotating disc with variable thickness.

Despite applications in different industries, piezoelectric materials have weaknesses, including fragility. Porous piezoelectric ceramics exhibit more softness and low density. Porous piezoelectric materials have various usages such as medical ultrasonic devices, under water acoustics, low frequency hydrophones, accelerometers, vibratory sensors, contact microphones, etc. [24, 25]. Li et al. [26] studied about the fabrication of porous piezoelectrics and porosity-graded piezoelectric actuators. Bowen et al. [27] studied about the fabrication and properties of porous piezoelectric materials with high hydrostatic property. Zielinski [28] discussed the fundamentals of multiphysics modeling of piezoporoelastic structures. Jabbari et al. [29, 30] studied the axisymmetric and non-axisymmetric mechanical and thermal stresses in FGPPM hollow cylinders. Meshkini et al. [31] presented a 2D stress analysis in 2D-FGPPM hollow cylinder in thermal environment.

Although the angular velocity of the rotating disc is usually constant during work, it may vary during the time. The disc may have an altering angular speed through the start and/or stop process. Clearly, it has an influence on the deformations and mechanical stresses in a rotating disc. Thus, investigation of rotating discs with variable angular velocity is vital. In all of the previously mentioned articles about rotating disc, the angular speed is assumed to be constant. Rotating discs with variable angular velocity were rarely studied in the literature just about FGM discs (not smart discs) and also without considering the magnetic field. Dai and Dai [32] used variable separation method to solve the governing differential equation of a uniform thickness FGM disc with variable angular speed. Moreover, they [33] investigated thermal stress in FGM discs with variable angular velocity. Zheng et al. [34] studied the effect of multiple thickness profile on displacement and stress distributions of FGM discs with variable angular speed. Recently, Salehian et al. [35] presented a procedure for calculation of the shear stress and tangential displacement in variable thickness rotating discs with varying angular velocity.

It is well-known that by using the power-law variation form, more general variation forms can be achieved rather than the exponential form for gradient of material properties of FGMs [36]. Besides, more desirable behavior was reported for FGMs with power-law form [37]. Particularly, to achieve the desired behavior, the effect of gradient index on the behavior of FGM cylindrical shell is more significant for power-law form [38]. So, the power-law variation form is more general and more applicable than exponential form for material properties of FGMs. However, to the best of the authors' knowledge, the analysis of variable angular velocity discs made of power-law functionally graded porous piezoelectric material under two dimensional Lorentz forces (the second term of Lorentz force exists because of variable angular velocity) has not yet been investigated. In the present study, for the first time, the numerical solution is presented for analysis of an orthotropic rotating FGPPM disc that is porous, has variable thickness and angular velocity and is subjected to Lorentz force. The obtained equations are solved numerically using Runge-Kutta and shooting methods.

2. Basic Formulation of the Problem

The problem is a fluid-saturated FGPPM disc polarized in the radius direction which rotates about z axis with variable angular speed. The cylindrical coordinate system (r, θ, z) with origin identical to the center of the disc is associated with the disc. As shown in Fig. 1, the inner and outer radii of the disc are r_i and r_o, respectively. The disc is placed in a constant magnetic field in the thickness direction. The profile of thickness is assumed as a power-law function of radius as:

$$h(r) = h_i + (h_o - h_i)\left(\frac{r - r_i}{r_o - r_i}\right)^s \tag{1}$$

Constitutive equations of an FGPPM disc in cylindrical coordinate system is [39]:

$$\sigma_r = c_{11}\varepsilon_r + c_{12}\varepsilon_\theta + c_{13}\varepsilon_z - e_{11}E_r - \alpha p \tag{2}$$
$$\sigma_\theta = c_{12}\varepsilon_r + c_{22}\varepsilon_\theta + c_{23}\varepsilon_z - e_{12}E_r - \alpha p \tag{3}$$
$$\sigma_z = c_{13}\varepsilon_r + c_{23}\varepsilon_\theta + c_{33}\varepsilon_z - e_{13}E_r - \alpha p \tag{4}$$
$$\tau_{r\theta} = c_{66}\gamma_{r\theta} - e_{26}E_\theta \tag{5}$$
$$D_r = e_{11}\varepsilon_r + e_{12}\varepsilon_\theta + e_{13}\varepsilon_z + \epsilon_1 E_r \tag{6}$$

We know that [40]:

$$E_r = -\frac{\partial\phi}{\partial r} \tag{7}$$

$$E_\theta = -\frac{1}{r}\frac{\partial\phi}{\partial\theta} \tag{8}$$

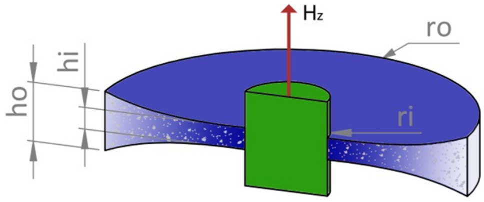

Fig. 1. FGPPM rotating disc in constant magnetic field.

Pore fluid pressure can be expressed as [41]:

$$p = (\xi - \alpha e)\mathcal{M} \tag{9}$$

where [41]:

$$\begin{aligned} \mathcal{M} &= \frac{K_u - K}{\alpha^2} \\ K_u &= K\left(1 + \frac{\alpha^2 K_f}{(1-\alpha)(\alpha-\varphi)K_f + \varphi K_f}\right) \\ e &= \varepsilon_r + \varepsilon_\theta + \varepsilon_z \end{aligned} \tag{10}$$

A key feature of the response of fluid-infiltrated porous material is the difference between undrained and drained deformation. These two modes of response represent limiting behaviors of the material: the undrained response characterizes the condition where the fluid is trapped in the porous solid such that $\zeta = 0$, while the drained response corresponds to zero pore pressure $p = 0$. For the undrained fluid condition where the fluid is trapped in the porous solid ($\xi = 0$), Eq. (9) becomes:

$$p = -\alpha e\mathcal{M} = \alpha\mathcal{M}(\varepsilon_r + \varepsilon_\theta + \varepsilon_z) \tag{11}$$

Substituting Eq. (11) into Eqs. (2), (3) and (4) leads to:

$$\begin{aligned} \sigma_r &= \bar{c}_{11}\varepsilon_r + \bar{c}_{12}\varepsilon_\theta + \bar{c}_{13}\varepsilon_z - e_{11}E_r \\ \sigma_\theta &= \bar{c}_{12}\varepsilon_r + \bar{c}_{22}\varepsilon_\theta + \bar{c}_{23}\varepsilon_z - e_{12}E_r \\ \sigma_z &= \bar{c}_{13}\varepsilon_r + \bar{c}_{23}\varepsilon_\theta + \bar{c}_{33}\varepsilon_z - e_{13}E_r \end{aligned} \tag{12}$$

where

$$\bar{c}_{ij} = c_{ij} + \alpha^2\mathcal{M} \tag{13}$$

A power-low function is taken for material properties variation as:

$$\begin{aligned} &\bar{c}_{ij} = \bar{c}_{ij0}r^\beta,\ e_{ij} = e_{ij0}r^\beta,\ \varepsilon_e = \varepsilon_{e0}r^\beta, \\ &\mu = \mu_0 r^\beta,\ \rho = \rho_0 r^\beta, \epsilon_1 = \epsilon_{10}r^\beta \end{aligned} \tag{14}$$

where zero subscript denotes corresponding material constants and β is the inhomogeneity index. Strains in terms of displacements can be written as [37]:

$$\begin{aligned} \varepsilon_r &= \frac{\partial u_r}{\partial r} \\ \varepsilon_\theta &= \frac{u_r}{r} + \frac{1}{r}\frac{\partial u_\theta}{\partial\theta} \\ \gamma_{r\theta} &= \frac{1}{r}\frac{\partial u_r}{\partial\theta} + \frac{\partial u_\theta}{\partial r} - \frac{u_\theta}{r} \end{aligned} \tag{15}$$

Because of symmetry of the problem relative to θ, none of variables depend on θ and all derivatives relative to θ is zero. So that, Eq. (8) becomes zero and Eq. (15) is simplified as:

$$\begin{aligned}\varepsilon_r &= \frac{\partial u_r}{\partial r}\\ \varepsilon_\theta &= \frac{u_r}{r}\\ \gamma_{r\theta} &= \frac{\partial u_\theta}{\partial r} - \frac{u_\theta}{r}\end{aligned} \tag{16}$$

Regarding plane stress condition ($\sigma_z = 0$), ε_z is calculated from Eq. (4). Then, by substituting Eqs. (16) and (11) into Eqs. (2) and (3), we have:

$$\sigma_r = c_1\frac{\partial u_r}{\partial r} + c_2\frac{u_r}{r} + e_1\frac{\partial \phi}{\partial r} \tag{17}$$

$$\sigma_\theta = c_2\frac{\partial u_r}{\partial r} + c_3\frac{u_r}{r} + e_2\frac{\partial \phi}{\partial r} \tag{18}$$

$$\tau_{r\theta} = c_{66}\left(\frac{\partial u_\theta}{\partial r} - \frac{u_\theta}{r}\right) \tag{19}$$

$$D_r = e_1\frac{\partial u_r}{\partial r} + e_2\frac{u_r}{r} - e_3\frac{\partial \phi}{\partial r} \tag{20}$$

where c_i and e_i $(i = 1, 2, 3)$ can be found in the appendix. A constant magnetic field is assumed. So, the perturbation of the magnetic field vector $\vec{h}$ is calculated as [42]:

$$\vec{h} = \nabla \times (\vec{u} \times \vec{H}) \tag{21}$$

where, $\vec{u} = (u_r, u_\theta, u_z)$ and $\vec{H} = (0, 0, H_z)$. The induced electric field $\vec{E}$ is calculated as [43]:

$$\begin{aligned}\vec{E} &= -\mu(\dot{\vec{u}} \times \vec{H}) = -\mu(\dot{u}_r, \dot{u}_\theta, \dot{u}_z) \times (0, 0, H_z)\\ &= -\mu H_z(\dot{u}_\theta, -\dot{u}_r, 0)\end{aligned} \tag{22}$$

The electric current density vector $\vec{J}$ becomes [43]:

$$\begin{aligned}\vec{J} &= \nabla \times \vec{h} - \varepsilon_e\frac{d\vec{E}}{dt} = \left(0, -\frac{\partial h_z}{\partial r}, 0\right)\\ &+ \varepsilon_e\mu H_z(\ddot{u}_\theta, -\ddot{u}_r, 0)\end{aligned} \tag{23}$$

The Lorentz body force can be calculated as [44, 45]:

$$\begin{aligned}\vec{f} &= \mu(\vec{J} \times \vec{H})\left[\mu\left(0, -\frac{\partial h_z}{\partial r}, 0\right)\right.\\ &\left. + \varepsilon_e\mu H_z(\ddot{u}_\theta, -\ddot{u}_r, 0)\right] \times (0, 0, H_z)\\ &= \mu\left[\left(-\frac{\partial h_z}{\partial r}H_z, 0, 0\right) + \varepsilon_e\mu H_z^2(-\ddot{u}_r, -\ddot{u}_\theta, 0)\right]\end{aligned} \tag{24}$$

Also:

$$\begin{aligned}\frac{\partial h_z}{\partial r} &= -\frac{\partial}{\partial r}\left(\frac{1}{r}\frac{\partial (ru_r)}{\partial r}\right) = -\frac{\partial}{\partial r}\left(\frac{\partial u_r}{\partial r} + \frac{u_r}{r}\right)\\ &= -\left(\frac{\partial^2 u_r}{\partial r^2} + \frac{1}{r}\frac{\partial u_r}{\partial r} - \frac{u_r}{r^2}\right)\end{aligned} \tag{25}$$

Substituting the term $\frac{\partial h_z}{\partial r}$, we have:

$$f_r = \mu H_z\left(\frac{\partial^2 u_r}{\partial r^2} + \frac{1}{r}\frac{\partial u_r}{\partial r} - \frac{u_r}{r^2}\right) - \varepsilon_e\mu^2 H_z^2\ddot{u}_r \tag{26}$$

$$f_\theta = -\varepsilon_e\mu^2 H_z^2\ddot{u}_\theta \tag{27}$$

Despite the cases that previously considered in the literature in which the Lorentz force has one component in the radial direction because of constant angular speed, the Lorentz force has two components in the radial as well as circumferential direction. The circumferential component is created because the disc rotates with angular acceleration. Equations of motion can be expressed as [34, 44]:

$$\frac{\partial (h\sigma_r)}{\partial r} + h\frac{\sigma_r - \sigma_\theta}{r} + h\rho r\omega^2 + hf_r = 0 \tag{28}$$

$$\frac{\partial (h\tau_{r\theta})}{\partial r} + \frac{2h\tau_{r\theta}}{r} - h\rho r\dot{\omega} + hf_\theta = 0 \tag{29}$$

Now, Eqs. (17) , (18) and (26) are substituted into Eq. (28), and Eqs. (19) and (27) are substituted into Eq. (29). So, we have:

$$\begin{aligned}&(hc_1 + h\mu H_z)\frac{\partial^2 u_r}{\partial r^2} + \left(c_1\frac{\partial h}{\partial r} + h\frac{\partial c_1}{\partial r} + \frac{hc_1}{r} + \frac{h\mu H_z}{r}\right)\frac{\partial u_r}{\partial r} + \left(\frac{c_2}{r}\frac{\partial h}{\partial r} + \frac{h}{r}\frac{\partial c_2}{\partial r} - \frac{hc_3}{r^2} - \frac{h\mu H_z}{r^2}\right)u_r\\ &+ (he_1)\frac{\partial^2 \phi}{\partial r^2} + \left(e_1\frac{\partial h}{\partial r} + h\frac{\partial e_1}{\partial r} + \frac{he_1}{r} - \frac{he_2}{r}\right)\frac{\partial \phi}{\partial r} + h\rho r\omega^2 - h\varepsilon_e\mu^2 H_z^2\ddot{u}_r = 0\end{aligned} \tag{30}$$

$$\begin{aligned}&(hc_{66})\frac{\partial^2 u_\theta}{\partial r^2} + \left(c_{66}\frac{\partial h}{\partial r} + h\frac{\partial c_{66}}{\partial r} + \frac{hc_{66}}{r}\right)\frac{\partial u_\theta}{\partial r} + \left(-\frac{c_{66}}{r}\frac{\partial h}{\partial r} - \frac{h}{r}\frac{\partial c_{66}}{\partial r} - \frac{hc_{66}}{r^2}\right)u_\theta\\ &- h\rho r\dot{\omega} - h\varepsilon_e\mu^2 H_z^2\ddot{u}_\theta = 0\end{aligned} \tag{31}$$

Electrostatic equation of axially symmetric disc is as:

$$\frac{\partial}{\partial r}(rhD_r) = 0 \tag{32}$$

Using Eq. (6), Eq. (32) can be rewritten as:

$$\begin{aligned}&(he_1)\frac{\partial^2 u_r}{\partial r^2} + \left(e_1\left(\frac{\partial h}{\partial r} + \frac{h}{r}\right) + h\frac{\partial e_1}{\partial r} + \frac{he_2}{r}\right)\frac{\partial u_r}{\partial r}\\ &+ \left(\frac{e_2}{r}\left(\frac{\partial h}{\partial r} + \frac{h}{r}\right) + \frac{h}{r}\frac{\partial e_2}{\partial r} - \frac{he_2}{r^2}\right)u_r + (he_3)\frac{\partial^2 \phi}{\partial r^2}\\ &+ \left(-e_3\left(\frac{\partial h}{\partial r} + \frac{h}{r}\right) - h\frac{\partial e_3}{\partial r}\right)\frac{\partial \phi}{\partial r} = 0\end{aligned} \tag{33}$$

The angular velocity of the disc is taken as an exponential function of time as:

$$\omega(t) = \omega_0 e^{-\lambda t} \tag{34}$$

where ω_0 and λ are both constant. Then, Eqs. (30), (31) and (33) become:

$$\begin{aligned}&A_0\frac{\partial^2 u_r}{\partial r^2} + A_1\frac{\partial u_r}{\partial r} + A_2 u_r + A_3\frac{\partial^2 \phi}{\partial r^2} + A_4\frac{\partial \phi}{\partial r}\\ &- h\varepsilon_e\mu^2 H_z^2 \ddot{u}_r + h\rho r\omega_0 e^{-2\lambda t} = 0\end{aligned} \tag{35}$$

$$\begin{aligned}&B_0\frac{\partial^2 u_\theta}{\partial r^2} + B_1\frac{\partial u_\theta}{\partial r} + B_2 u_\theta - h\varepsilon_e\mu^2 H_z^2 \ddot{u}_\theta\\ &+ h\rho r\omega_0\lambda e^{-\lambda t} = 0\end{aligned} \tag{36}$$

$$C_0\frac{\partial^2 u_r}{\partial r^2} + C_1\frac{\partial u_r}{\partial r} + C_2 u_r + C_3\frac{\partial^2 \phi}{\partial r^2} + C_4\frac{\partial \phi}{\partial r} = 0 \tag{37}$$

where A_i, B_i, and C_i are given in the appendix.

3. The Solution of Derived Equations

Using the method of separation of variables, u_r, u_θ and ϕ can be written as [32, 34]:

$$\begin{aligned}u_r &= u_r(r,t) = U_r(r)e^{-2\lambda t}\\ u_\theta &= u_\theta(r,t) = U_\theta(r)e^{-\lambda t}\\ \phi &= \phi(r,t) = \Phi(r)e^{-2\lambda t}\end{aligned} \tag{38}$$

First, Eq. (38) is substituted into (30), (31) and (33), then time terms are eliminated. So, the following equations are obtained:

$$\begin{aligned}&A_0 U_r'' + A_1 U_r' + (A_2 - 4h\varepsilon_e\mu^2 H_z^2\lambda^2)U_r + A_3\Phi''\\ &\quad + A_4\Phi' + h\rho r\omega_0^2 = 0\end{aligned} \tag{39}$$

$$\begin{aligned}&B_0 U_\theta'' + B_1 U_\theta' + (B_2 - h\varepsilon_e\mu^2 H_z^2\lambda^2)U_\theta\\ &\quad + h\rho r\lambda\omega_0 = 0\end{aligned} \tag{40}$$

$$C_0 U_r'' + C_1 U_r' + C_2 U_r + C_3\Phi'' + C_4\Phi' = 0 \tag{41}$$

where $(\ )'$ and $(\ )''$ indicate $\frac{d}{dr}$ and $\frac{d^2}{dr^2}$, respectively. The disc is assumed to be in the fixed-free mechanical boundary condition. So:

$$\begin{aligned}u_r\Big|_{r=r_i} &= 0\\ u_\theta\Big|_{r=r_i} &= 0\end{aligned} \tag{42}$$

$$\begin{aligned}\sigma_r\Big|_{r=r_o} &= 0\\ \tau_{r\theta}\Big|_{r=r_o} &= 0\end{aligned} \tag{43}$$

Eqs. (38) are substituted into Eq. (42), then by the elimination of time terms it becomes:

$$\begin{aligned}U_r(r_i) &= 0\\ U_\theta(r_i) &= 0\end{aligned} \tag{44}$$

Eqs. (17) and (19) are substituted into Eq. (43). Then time terms are eliminated and we have:

$$\begin{aligned}&c_1(r_o)U_r'(r_o) + c_1(r_o)\frac{U_r(r_o)}{r_o} = e_1(r_o)\varphi'(r_o)\\ &U_\theta'(r_o) = \frac{U_\theta(r_o)}{r_o}\end{aligned} \tag{45}$$

For electric boundary conditions, the electric potential at inner and outer radii at time zero is assumed as:

$$\begin{aligned}\Phi(r_i) &= \Phi_i\\ \Phi(r_o) &= \Phi_o\end{aligned} \tag{46}$$

Eqs. (39), (40) and (41) are three coupled second-order ordinary differential equations (with variable coefficient) which can be solved by Runge-Kutta method. The boundary conditions of these equations are given in Eqs. (44), (45) and (46). By the combination of Eqs. (39) and (41), U_r'' and ϕ'' are calculated as:

$$\begin{aligned}\Phi'' &= f_1 U_r' + f_2 U_r + f_3\Phi' + f_4\\ U_r'' &= g_1 U_r' + g_2 U_r + g_3\Phi' + g_4\end{aligned} \tag{47}$$

where f_i and g_i are available in the appendix. Besides, U_θ'' is obtained from Eq. (40) as follows:

$$U_\theta'' = h_1 U_\theta' + h_2 U_\theta + h_3 \tag{48}$$

where h_i are available in the appendix. Then, Eqs. (47) and (48) should be converted to a new form in order to use Runge-Kutta method. So, we have:

$$\begin{aligned}q_2' &= U_r'' = g_1 q_2 + g_2 q_1 + g_3 q_4 + g_4\\ q_4' &= \Phi'' = f_1 q_2 + f_2 q_1 + f_3 q_4 + f_4\\ q_6' &= U_\theta'' = h_1 q_6 + h_2 q_5 + h_3\end{aligned} \tag{49}$$

where:

$$
\begin{aligned}
q_1 &= U_r \\
q_2 &= U_r' \\
q_3 &= \Phi \\
q_4 &= \Phi' \\
q_5 &= U_\theta \\
q_6 &= U_\theta'
\end{aligned}
\tag{50}
$$

where:

$$
[\vec{F}] = \begin{bmatrix} q_2 \\ g_1 q_2 + g_2 q_1 + g_3 q_4 + g_4 \\ q_4 \\ f_1 q_2 + f_2 q_1 + f_3 q_4 + f_4 \\ q_6 \\ h_1 q_6 + h_2 q_5 + h_3 \end{bmatrix} \tag{51}
$$

The resulted equations can be solved using the fourth-order Runge-Kutta method which is expressed as:

$$
\vec{q}(r+\Delta r) = \vec{q}(r) + \frac{1}{6}(\vec{K}_1 + 2\vec{K}_2 + 2\vec{K}_3 + \vec{K}_4) \tag{52}
$$

where $\vec{K}_1$, $\vec{K}_2$, $\vec{K}_3$ and $\vec{K}_4$ are expressed as:

$$
\begin{aligned}
\vec{K}_1 &= \Delta r \vec{F}(r, \vec{q}) \\
\vec{K}_2 &= \Delta r \vec{F}\left(r + \frac{\Delta r}{2}, \vec{q} + \frac{\vec{K}_1}{2}\right) \\
\vec{K}_3 &= \Delta r \vec{F}\left(r + \frac{\Delta r}{2}, \vec{q} + \frac{\vec{K}_2}{2}\right) \\
\vec{K}_4 &= \Delta r \vec{F}(r + \Delta r, \vec{q} + \vec{K}_3)
\end{aligned}
\tag{53}
$$

where Δr is step size and $\vec{q}$ is a vector which contains q_i. Employing boundary Eqs. (44) and (46) in Eq. (49), at the inner radii we have:

$$
q_1 = 0,\ q_3 = \Phi_i,\ q_5 = 0 \tag{54}
$$

Also, q_2, q_4, q_6 at inner radii are unknown. Employing boundary Eqs. (45) and (46) in Eq. (49), at outer radii we have:

$$
\begin{aligned}
& c_1(r_o) q_2 + c_2(r_o)\frac{q_1}{r_o} - e_1(r_o) q_4 = 0 \\
& q_6 - \frac{q_5}{r_o} = 0, \\
& q_3 - \Phi_o = 0
\end{aligned}
\tag{55}
$$

Since Runge-Kutta method is an initial value method, all of $q_1, q_2, \cdots, q_6$ should be known at inner radius. But in this case q_2, q_4, q_6 are unknown. So, by using the shooting method, these unknown values are guessed. Then, equations are solved by Runge-Kutta method, and calculated qi at outer boundary condition is substituted in the outer boundary Eq. (55). If outer boundary conditions are satisfied, the problem is solved. Otherwise, new guess should be made in order to satisfying outer boundary conditions. It should be mentioned that the error of method depends on the ODE solver method, which in this case is 4th-order Runge-Kutta. In this method, the total accumulated error is on the order of $o(\Delta r^4)$ [46]. For numerical calculation of this article Δr is selected to be $0.01(r_o - r_i)$.

4. Numerical Results and Discussion

In this section numerical results are depicted for studying the influence of effective parameters on the mechanical behavior of the disc. The following non-dimensional parameters are used as:

$$
R = \frac{r - r_i}{r_o - r_i}, \quad u^* = \frac{u}{r_i}, \quad \sigma^* = \frac{\sigma}{c_{110}}, \quad \phi^* = \sqrt{\frac{\epsilon_{10}}{c_{110}}}\frac{\phi}{r_o}
$$

4.1. Validation

Since there is not any reported research about smart disc with variable angular velocity, to validate the numerical process, the result for an isotropic FGM disc with variable thickness and angular velocity is compared with reported work by Zheng et al. [34]. The material properties are taken as a power-law function; however the thickness profile is considered as an exponential function. Details and material properties can be found in Zheng et al. [34]. Furthermore, the radial displacement and radial stress is compared with rotating FGPM disc reported by Ghorbanpour Arani et al. [46]. In this case: $\Omega = 1$, $\mu = 1.3$, $N = 1$ and other details and material properties can be found in Ghorbanpour Arani et al. [47]. As shown in Fig. 2, results show good agreement.

4.2. Investigation of Effective Parameters

In this part, the inner and outer radii of the disc are considered as $r_i = 0.05$m and $r_o = 0.25$m, and inner and outer thickness are taken $h_i = 0.05$m and $h_o = 0.15$m, respectively. Moreover, the electric boundary conditions are assumed as: $\Phi_i = 0$ and $\Phi_o = 500$V. In all numerical simulations, unless otherwise stated, it is considered that: $s = 2$, $\omega_0 = 50\pi$, $\lambda = 0.5$, $\beta = 1.5$, $\varphi = 0.02$ and $H^* = 1$ ($H_z = H^* \times 10^2$A/m) [48, 49]. The used material constants are listed in Table 1 [41].

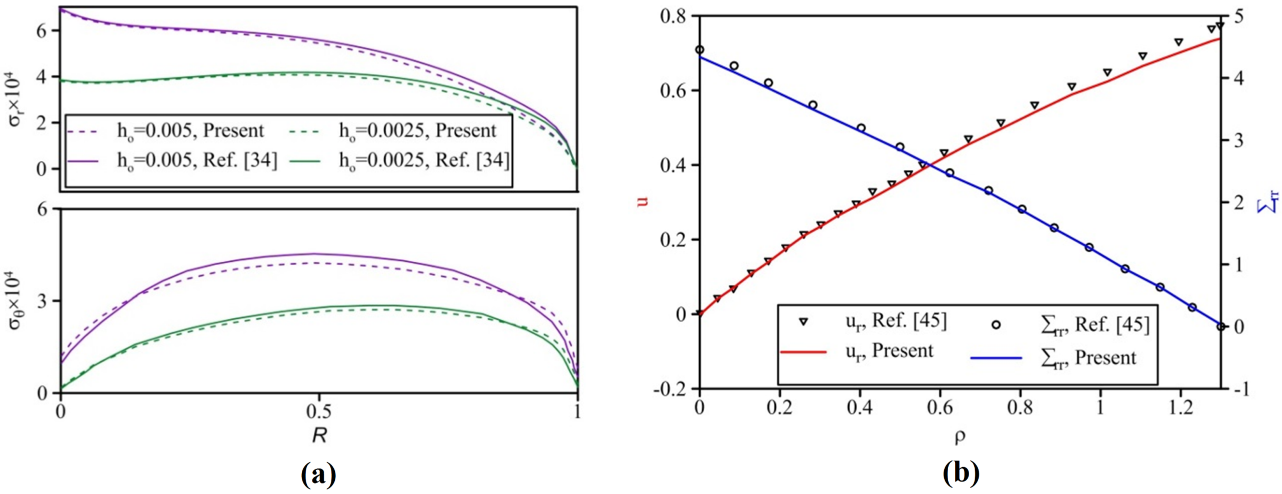

Fig. 2. Validation of results with a) An FGM variable thickness and angular velocity rotating disc, and b) A piezoelectric rotating disc.

Table 1
Material constants.

c_{110}(MPa)	115
c_{120}	74
c_{130}	74
c_{220}	139
c_{230}	78
c_{330}	139
c_{660}	25.6
e_{110}(C/m^2)	15.1
e_{120}	-5.2
e_{130}	-5.2
g_{110}(C^2/Nm^2)	5.6×10^{-9}
ρ_0(kg/m^3)	7500
K	35×10^9
K_f	3300
α	0.27
ε_0	$4\pi\times10^{-5}$
μ_0	8.85×10^{-6}

Case 1:
In this case the influence of grading index on the stresses, displacement and electromagnetic potential of the disc is investigated. Figs. 3a, 3b and 3c illustrate that using functionally graded piezoelectric (FGPM) yields in reducing the stresses. Additionally, by increasing the grading index, stresses decrease at a decreasing rate. Figs. 3d and 3e show that employing FGPM results in an increase in radial and circumferential displacements. Radial and circumferential displacements rise by an increase in inhomogeneity index. So, in practical usages of piezoelectric disc, larger displacements together with smaller stresses can be achieved by using functionally graded piezoelectric. Fig. 3f indicates that increasing in yields in an increase in the maximum electric potential. Besides, as seen in Figs. 3a, 3c-3f, the electro-mechanical boundary conditions are satisfied completely. It should be noted that the equations are nonlinear functions of the inhomogeneity index. Therefore, the response of the FGPPM disc shows no regular variation by altering the inhomogeneity index

Case 2:
The effect of porosity on the behavior of the disc is investigated in this case. More investigations show that the effect of porosity on the shear stress as well as displacements is not considerable. So, for the sake of brevity, the radial stress and hoop stress are demonstrated in Fig. 4. According to Fig. 4, both radial and hoop stress increase by rise in the porosity.

Case 3:
In this case, the effect of magnetic field on the response of the disc is analyzed. Figs. 5a and 5b show that an increase in the magnetic field can reduce the radial and hoop stresses. Fig. 5c depicts that shear stress is decreased as a result of an increase in magnetic field and this reduction is more significant at the inner radius. As demonstrated in Figs. 5d and 5e, an increase in the magnetic field causes reduction in the both radial and circumferential displacement. Fig. 5f indicates that maximum electric potential decreases by increase in the magnetic field. It can be concluded that with applying magnetic field, more stresses caused by environmental effects can be applied. It is worth mentioning that, as before mentioned in the literature review, angular velocity is assumed to be constant in most of the reported works about the piezoelectric rotating disc. Considering this assumption results in omitting the $\ddot{u}_r$ and $\ddot{u}_\theta$. Hence, the circumferential Lorentz force and the second term of radial Lorentz force in Eq. (27) are omitted and applying magnetic field has no effect on the shear stress. Conversely, in this research, the shear stress is affected by the magnetic field as a result of considering the angular acceleration.

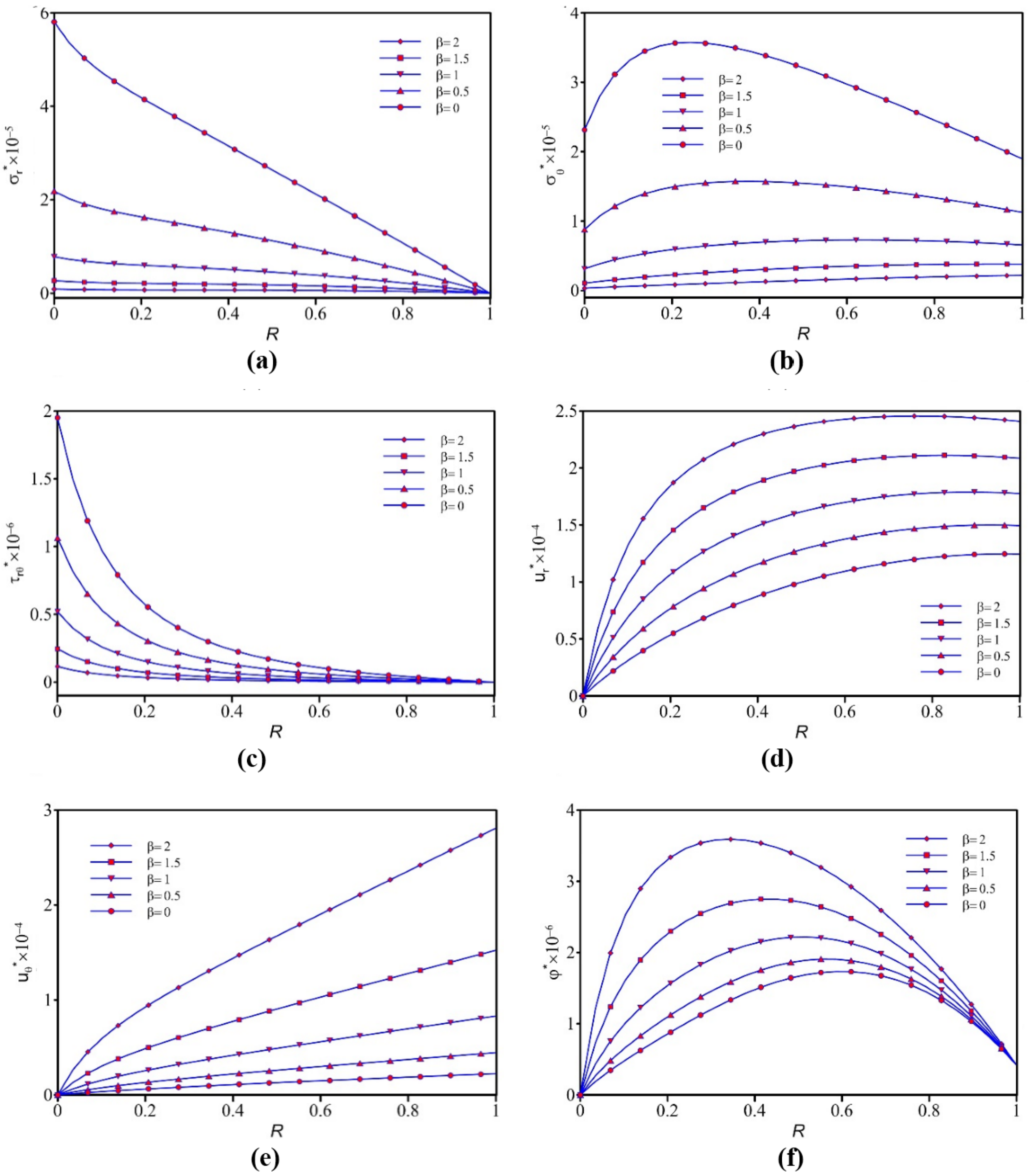

Fig. 3. Effect of grading index on the a) Radial stress, b) Hoop stress, c) Shear stress, d) Radial displacement, e) Circumferential displacement, and f) Electric potential distributions.

The following explanation may help for better clearance about the effect of magnetic field behavior of the disc. First of all, it should be noticed that there are interactions between magnetic, electric and elastic fields in the disc. So, the behavior of the disc is complicated and the effect of all parameters must be considered simultaneously. As known, the Lorentz force is created as a result of a movement of a particle in a magnetic field. By existence of a magnetic field, existing $u_r, \ddot{u}_r$ and $\ddot{u}_\theta$ result in creating Lorentz forces in the both radial and circumferential directions. Then, these forces affect the stresses and displacements. It should be noted that all of the parameters that affect the radial displacement are effective on the magnitude of the Lorentz force.

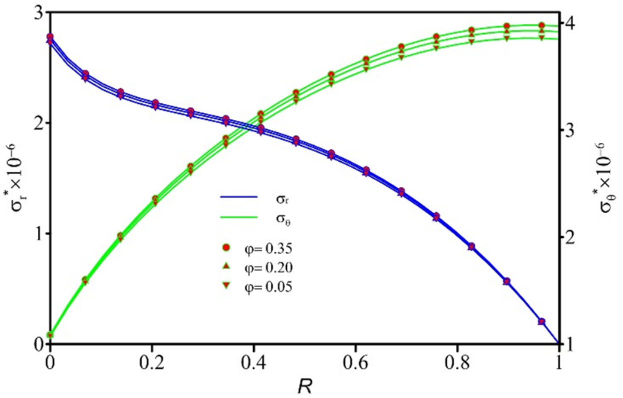

Fig. 4. Effect of porosity on the radial stress and hoop stress.

By changing each of these parameters (such as thickness, boundary condition and direction of displacement) the effect of the Lorentz force on the behavior of smart structure may be affected. So, an accurate explanation about the magnetic field effect on the smart structures is complicated.

Case 4:
Initial angular velocity is the next parameter that its effect on the stresses and displacements of the disc is studied. Fig. 6a illustrates that both radial and hoop stresses increase as initial angular speed increases. In addition, the maximum of radial and hoop stresses occurs at inner and outer boundaries, respectively. Fig. 6b shows that as angular speed increases, the shear stress increases. Form Fig. 6c, it can be seen that radial and circumferential displacements increase with a rise in angular speed. Moreover, the maximum electric potential increases by increase in initial angular speed. Therefore, it can be concluded that an increase in angular speed results in a rise in stresses and displacements of the disc.

Case 5:
The profile of thickness is the next effective parameter that is studied now. The stresses and displacements of a disc with different profile of thickness are demonstrated in Fig. 7. The boundary condition and assumed parameters are kept as before. In this case two types of discs with different thickness index are investigated: one disc with $h_i/h_o = 3$ and one with $h_o/h_i = 3$. For both cases, the thickness index is considered to be $s = 1, 2, 3$. The thickness profile of each disc can be seen in Fig. 8.

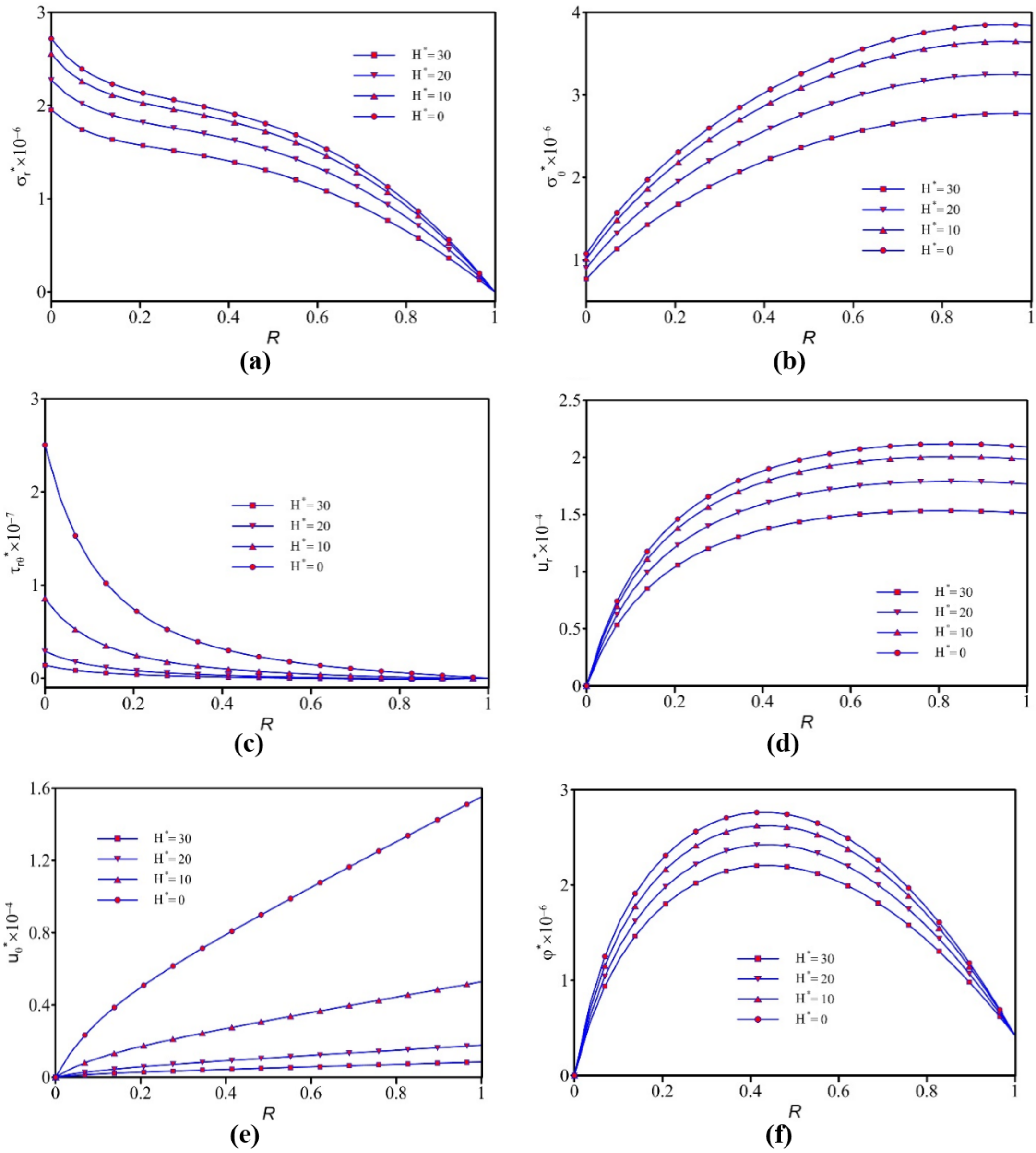

Fig. 5. Effect of magnetic field on the a) Radial stress, b) Hoop stress, c) Shear stress, d) Radial displacement, e) Circumferential displacement, and f) Electric potential distributions.

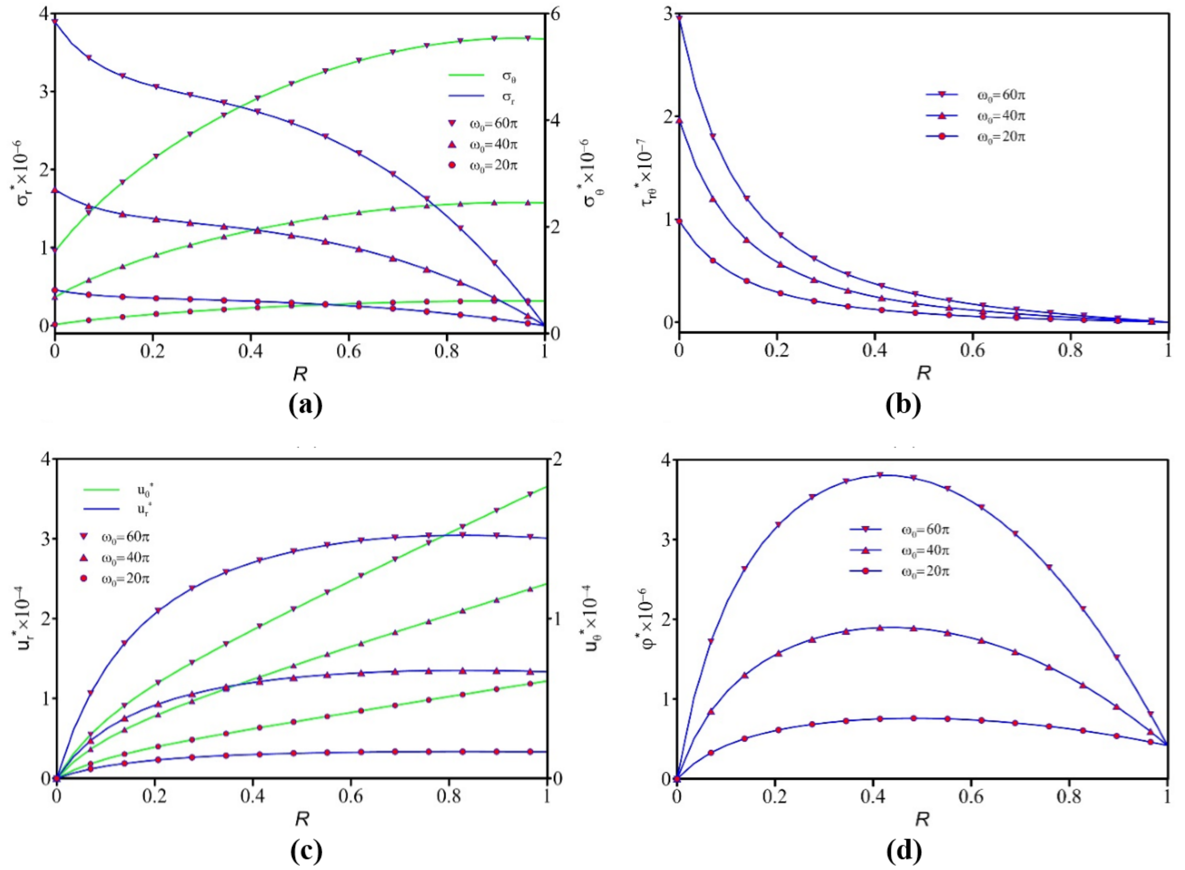

Fig. 6. Effect of initial angular speed on a) Radial and hoop stresses, b) Shear stress, c) Radial and circumferential displacements, and d) Electric potential distributions.

From Figs. 7a, 7b, and 7c can be concluded that increasing thickness index, increases stresses for $h_i > h_o$. Conversely, rise in thickness index reduces stresses for $h_o > h_i$. According to Figs. 7d and 7e, it can be seen that increasing thickness index increases both radial and circumferential displacements for $h_i > h_o$, while the effect of thickness index is vice versa for $h_o > h_i$. From Fig. 7, it can be concluded that using a disc with larger inner thickness and smaller outer thickness with smaller thickness index ($s = 1$) results in a reduction in stresses and displacements.

Case 6:

For the last case, the effect of the angular velocity function on the behavior of the disc is studied comprehensively. First of all, the effect of λ on angular speed as a function of time can be seen in Fig. 9. It shows that by increasing λ, the speed of reduction (deceleration) experiences an increase. Figs. 10 and 11 illustrate the effect of angular speed constant (λ) in two cases. For the first case, the effect of λ is investigated for the disc that is placed in a magnetic field ($H^* = 10$). It is obvious from Fig. 10 that λ has a significant effect on displacements and stresses of the disc. An increase in λ decreases stresses in the disc as shown in Figs. 10a, 10b and 10c. Furthermore, an increase in λ reduces both radial and circumferential displacements as shown in Figs. 10d and 10e. Therefore, it can be concluded that the disc with larger reduction acceleration (deceleration) of rotation speed has smaller stresses and displacement.

The second case is similar to the first case except the magnetic field is not applied. Investigations show that λ has a significant effect on circumferential displacement and shear stress, while its effect on radial displacement as well as radial and hoop stresses is negligible. So, the distributions of shear stress and circumferential stress are demonstrated in Fig. 11. From Fig. 11, rise in λ increases circumferential displacement and shear stress. This behavior is in contrast with the previous case. It is valuable to explore this behavior more carefully.

According to Eqs. (39), (40) and (41), by considering $H_z = 0$, the terms containing H_z corresponding Lorentz force (F_r and F_θ) become zero. Thus, λ is omitted from Eqs. (39) and (41). Since the Eq. (40) is decoupled from two other equations, this means that λ has no effect on radial displacement, electric potential, radial stress and hoop stress (radial and hoop stress are functions of radial displacement and electric potential according to Eqs. (17) and (18)). Conversely, λ is not omitted from Eq. (40) and it affects circumferential displacement and shear stress (because shear stress is

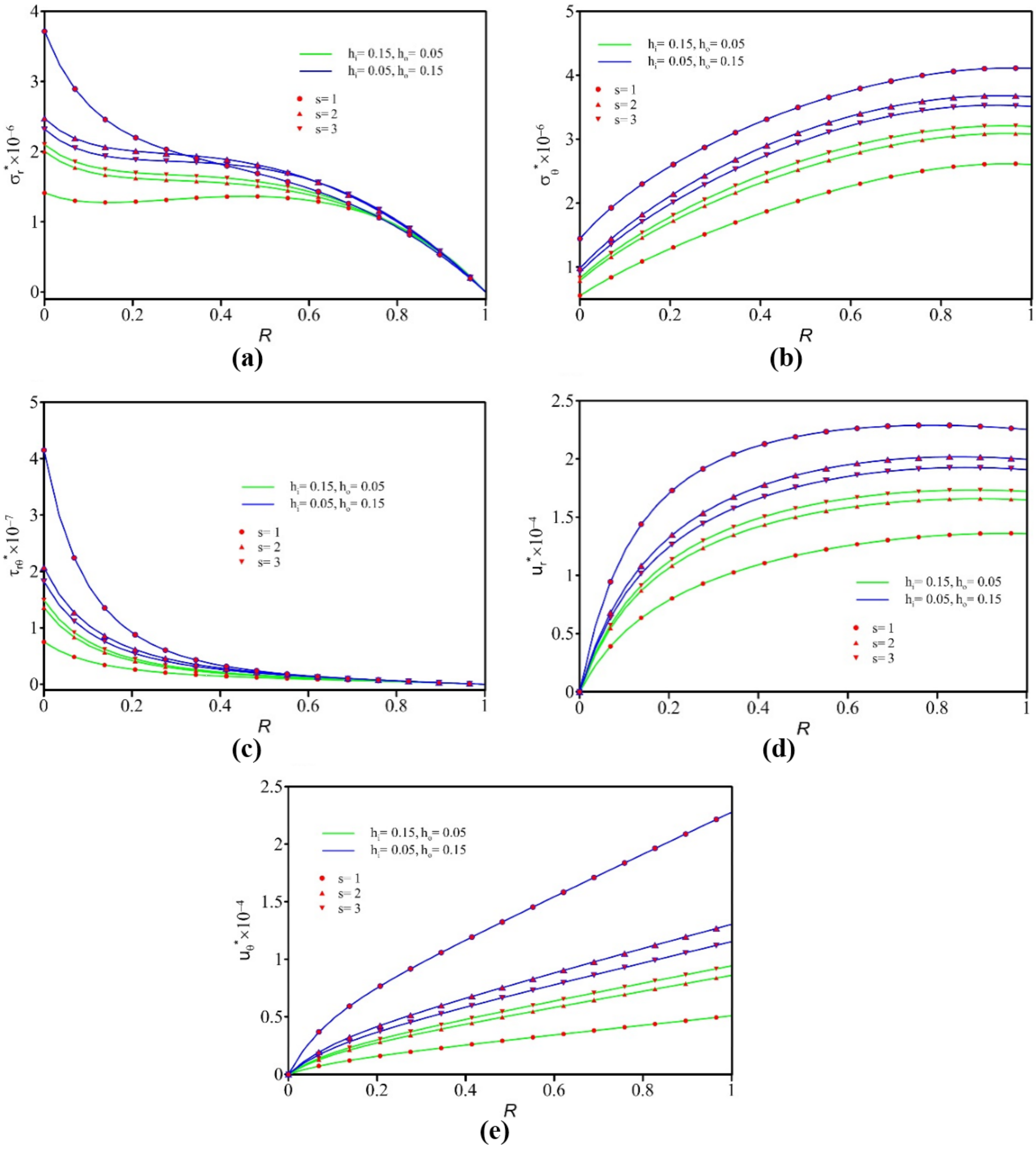

Fig. 7. Effect of thickness profile on the a) Radial stress, b) Hoop stress, c) Shear stress, d) Radial displacement, and e) Circumferential displacement distributions.

a function of circumferential displacement according to Eq. (19)). On the other hand, for the case that $H_z \neq 0$, the terms containing H_z corresponding Lorentz force (F_r and F_θ) are not omitted and λ remains in each three equations and affects stresses and displacements. So, considering or omitting the constant magnetic field creates a significant difference for behavior analysis of a rotating disc with angular acceleration. As before mentioned, the magnetic field was not considered for rotating disc with angular acceleration in the literature.

At last, 3D illustrations of stresses and displacement through the time are presented in Fig. 12. It is obvious that all boundary conditions are satisfied through the time. It can be concluded that time does not affect the position of maximums of the studied parameters.

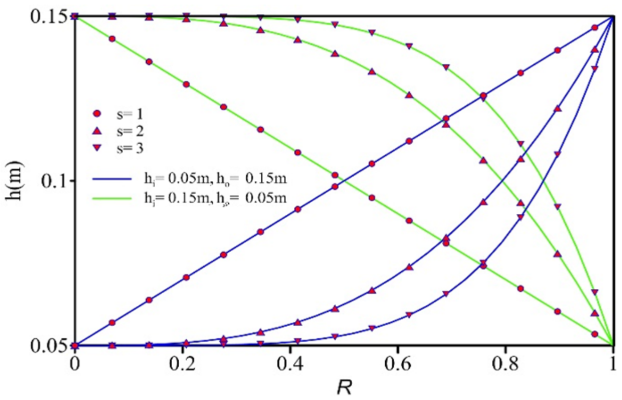

Fig. 8. Effect of thickness profile on the shape of the disc.

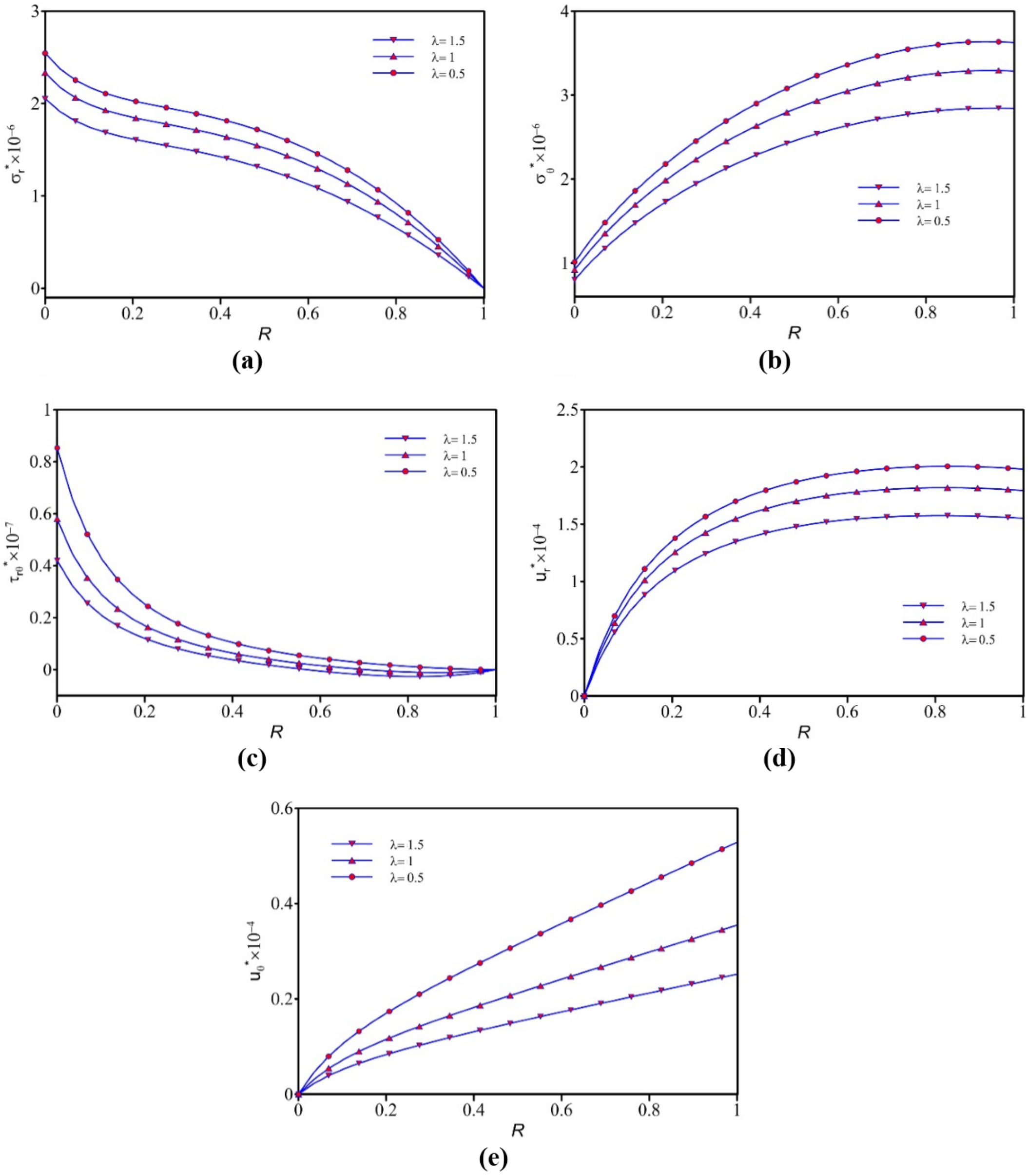

Fig. 9. Effect of angular speed constant (in the presence of magnetic field) on the a) Radial stress, b) Hoop stress, c) Shear stress, d) Radial displacement, and e) Circumferential displacement distributions.

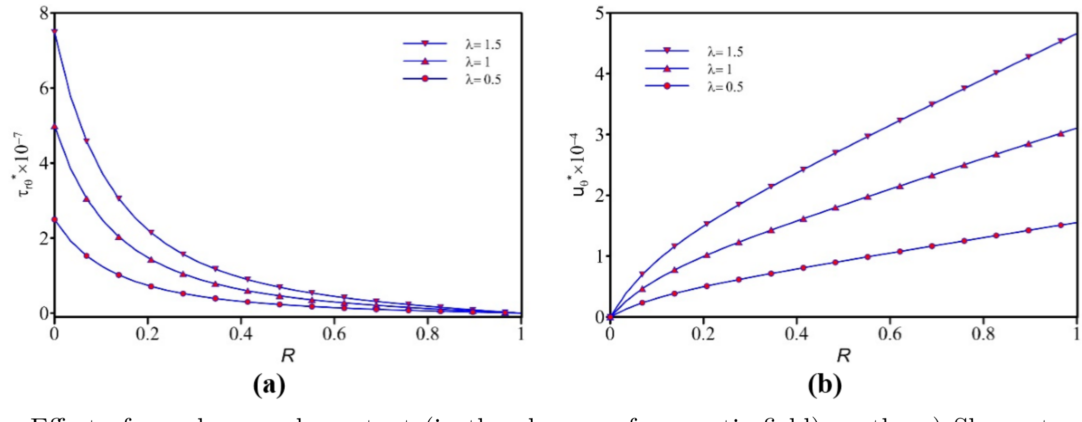

Fig. 10. Effect of angular speed constant (in the absence of magnetic field) on the a) Shear stress, and b) Circumferential displacement distributions.

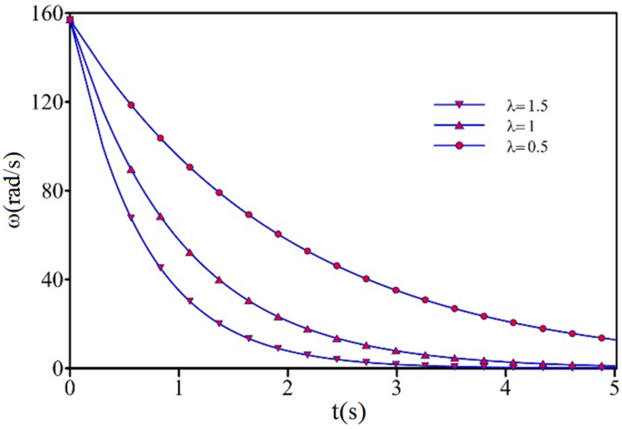

Fig. 11. Angular velocity function.

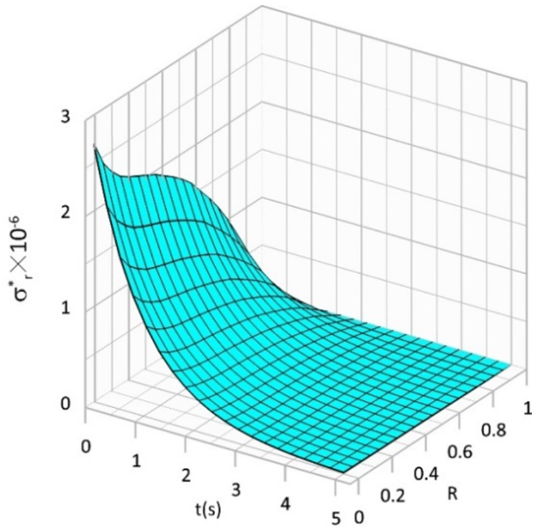

(a)

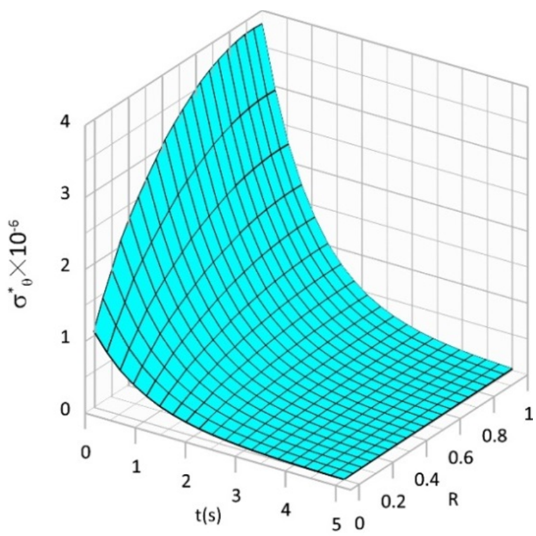

(b)

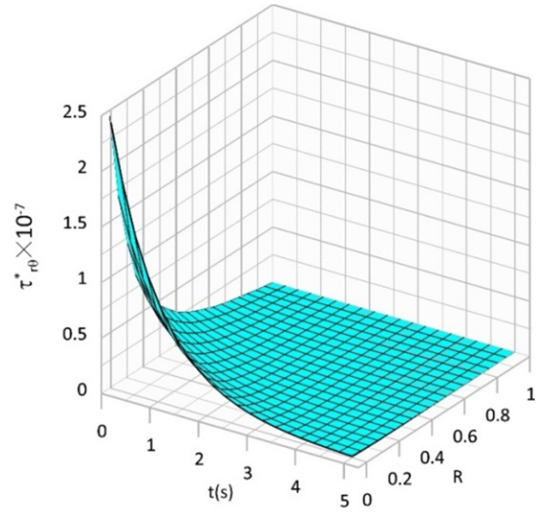

(c)

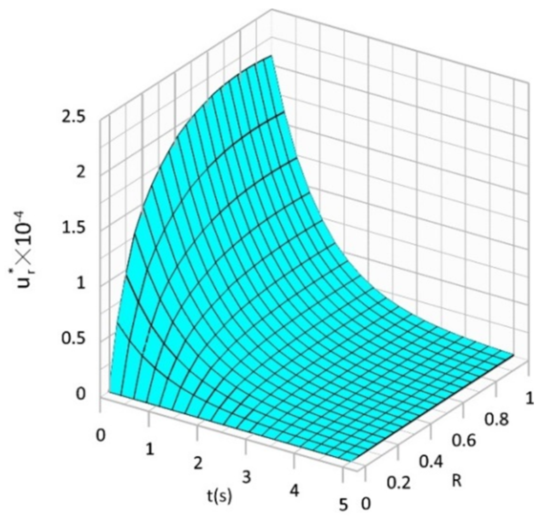

(d)

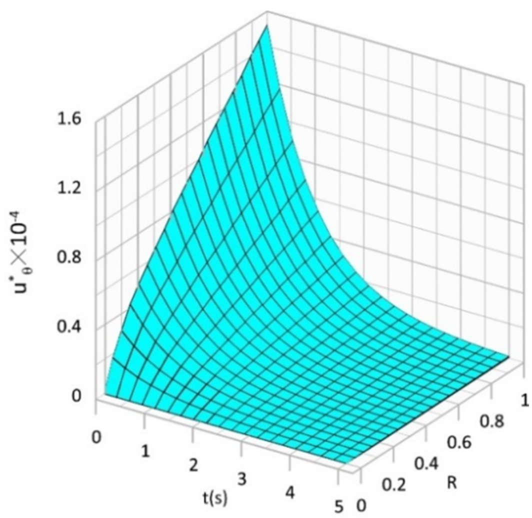

(e)

Fig. 12. Distribution of the a) Radial stress, b) Hoop stress, c) Shear stress, d) Radial, and e) Circumferential displacements for various rotating speed.

5. Conclusions

The stress and displacement of a rotating disc with angular acceleration and variable thickness made of a fluid-saturated porous functionally graded piezoelectric material which placed in a constant magnetic field were analyzed. Owing to angular acceleration, the disc was subjected to Lorentz force both radially and circumferentially. The material properties of the disc were supposed to obey radially power-law function. The disc was uniformly porous and its thickness varied as a function of radius. First, the resulted differential equations were converted to ordinary differential equations using the separation of variable technique. Then, obtained equations were solved by means of Runge-Kutta and shooting methods. The resulted conclusions can be summarized as:

- The shear stress is affected by the magnetic field as a result of considering the angular acceleration. An increase in the magnetic field results in a reduction in stresses and displacements.
- Considering or omitting the constant magnetic field creates a significant different for behavior analysis of a rotating disc with angular acceleration.
- By considering $H_z = 0$, radial displacement, electric potential, radial stress and hoop stress are independent of angular velocity constant (λ). Conversely, for the case that $H_z \neq 0$, the angular velocity constant (λ) has a considerable effect on radial and hoop stresses as well as radial and circumferential displacements.
- Using a disc with larger inner thickness and smaller outer thickness with smaller thickness index (s=1) results in a reduction in stresses and displacements.
- Larger displacements together with smaller stresses can be achieved by using functionally graded piezoelectric. Additionally, an increase in inhomogeneity index increases displacements and reduces stresses.
- Both radial and hoop stresses increase by rise in the porosity. More investigations show that the effect of porosity on the shear stress as well as displacements is negligible.
- An increase in angular speed results in a rise in stresses and displacements of the disc.

Appendix

In Eqs. (17)-(20), we have:

$$c_1 = \left(\bar{c}_{11} - \frac{\bar{c}_{13}^2}{\bar{c}_{33}}\right)$$

$$c_2 = \left(\bar{c}_{12} - \frac{\bar{c}_{13}\bar{c}_{23}}{\bar{c}_{33}}\right)$$

$$c_3 = \left(\bar{c}_{22} - \frac{\bar{c}_{23}^2}{\bar{c}_{33}}\right)$$

$$e_1 = \left(e_{11} - \frac{c_{13}e_{13}}{\bar{c}_{33}}\right)$$

$$e_2 = \left(e_{12} - \frac{\bar{c}_{23}e_{13}}{\bar{c}_{33}}\right)$$

$$e_3 = \left(\frac{e_{13}^2}{\bar{c}_{33}} + \epsilon_1\right)$$

In Eq. (35), we have:

$$A_0 = (hc_1 + h\mu H_z)$$

$$A_1 = \left(c_1\frac{\partial h}{\partial r} + h\frac{\partial c_1}{\partial r} + \frac{hc_1}{r} + \frac{h\mu H_z}{r}\right)$$

$$A_2 = \left(\frac{c_2}{r}\frac{\partial h}{\partial r} + \frac{h}{r}\frac{\partial c_2}{\partial r} - \frac{hc_3}{r^2} - \frac{h\mu H_z}{r^2}\right)$$

$$A_3 = (he_1)$$

$$A_4 = \left(e_1\frac{\partial h}{\partial r} + h\frac{\partial e_1}{\partial r} + \frac{he_1}{r} - \frac{he_2}{r}\right)$$

In Eq. (36), we have:

$$B_0 = (hc_{66})$$

$$B_1 = \left(c_{66}\frac{\partial h}{\partial r} + h\frac{\partial c_{66}}{\partial r} + \frac{hc_{66}}{r}\right)$$

$$B_2 = \left(-\frac{c_{66}}{r}\frac{\partial h}{\partial r} - \frac{h}{r}\frac{\partial c_{66}}{\partial r} - \frac{hc_{66}}{r^2}\right)$$

In Eq. (37), we have:

$$C_0 = (he_1)$$

$$C_1 = \left(e_1\left(\frac{\partial h}{\partial r} + \frac{h}{r}\right) + h\frac{\partial e_1}{\partial r} + \frac{he_2}{r}\right)$$

$$C_2 = \left(\frac{e_2}{r}\left(\frac{\partial h}{\partial r} + \frac{h}{r}\right) + \frac{h}{r}\frac{\partial e_2}{\partial r} - \frac{he_2}{r^2}\right) = \left(\frac{e_2}{r}\frac{\partial h}{\partial r} + \frac{h}{r}\frac{\partial e_2}{\partial r}\right)$$

$$C_3 = (-he_3)$$

$$C_4 = \left(-e_3\left(\frac{\partial h}{\partial r} + \frac{h}{r}\right) - h\frac{\partial e_3}{\partial r}\right)$$

In Eq. (48), we have:

$$h_1 = -B/B_0$$

$$h_2 = -(B_2 - h\varepsilon_e \mu^2 H_z^2 \lambda^2)/B_0$$

$$h_3 = -\rho r \lambda w_0/B_0$$

In Eq. (47), f_i and g_i are

$$f_0 = \left(\frac{A_0 C_3}{C_0} - A_3\right)$$

$$f_1 = \left(A_1 - \frac{A_0 C_1}{C_0}\right)/f_0$$

$$f_2 = \left(A_2 - \frac{A_0 C_2}{C_0} - 4h\varepsilon_e \mu^2 H_z^2 \lambda^2\right)/f_0$$

$$f_3 = \left(A_4 - \frac{A_0 C_4}{C_0}\right)/f_0$$

$$f_4 = h\rho r w_0^2/f_0$$

$$g_0 = \left(\frac{A_3 C_0}{C_3} - A_0\right)$$

$$g_1 = \left(A_1 - \frac{A_3 C_1}{C_3}\right)/g_0$$

$$g_2 = \left(A_2 - \frac{A_3 C_2}{C_3} - 4h\varepsilon_e \mu^2 H_z^2 \lambda^2\right)/g_0$$

$$g_3 = \left(A_4 - \frac{A_3 C_4}{C_3}\right)/g_0$$

$$g_4 = h\rho r w_0^2/g_0$$

References

[1] M. Shaban, H. Mazaheri, Closed-form elasticity solution for smart curved sandwich panels with soft core, Appl. Math. Modell., 76 (2019) 50-70.

[2] M. Shaban, A. Alibeigloo, Global bending analysis of corrugated sandwich panels with integrated piezoelectric layers, J. Sandwich Struct. Mater., 22(4) (2018) 1055-1073.

[3] M.J. Khoshgoftar, A. Ghorbanpour Arani, M. Arefi, Thermoelastic analysis of a thick walled cylinder made of functionally graded piezoelectric material, Smart Mater. Struct., 18(11) (2009) 115007.

[4] M. Saadatfar, Analytical solution for the creep problem of a rotating functionally graded magneto-electro-elastic hollow cylinder in thermal environment, Int. J. Appl. Mech., 11(06) (2019) 1950053.

[5] M. Saadatfar, M. Aghaie-Khafri, On the behavior of a rotating functionally graded hybrid cylindrical shell with imperfect bonding subjected to hygrothermal condition, J. Therm. Stresses, 38(8) (2015) 854-881.

[6] M. Saadatfar, Effect of hygrothermal environmental conditions on the time-dependent creep response of functionally graded magneto-electro-elastic hollow sphere, J. Stress Anal., 4(1) (2019) 27-41.

[7] A.M. Zenkour, Analytical solution for rotating exponentially-graded annular disks with various boundary conditions, Int. J. Struct. Stab. Dyn., 5(4) (2005) 557-557.

[8] H. Zharfi, Creep relaxation in FGM rotating disc with nonlinear axisymmetric distribution of heterogeneity, Theor. Appl. Mech. Lett., 9(6) (2019) 382-390.

[9] H. Zharfi, H. Ekhteraei Toussi, Time dependent creep analysis in thick FGM rotating disk with two-dimensional pattern of heterogeneity, Int. J. Mech. Sci., 140 (2018) 351-360.

[10] M. Saadatfar, Multiphysical time-dependent creep response of FGMEE hollow cylinder in thermal and humid environment, Mech. Time-Depend. Mater., (2019), DOI:10.1007/s11043019094330.

[11] H.L. Dai, Z.Q. Zheng, T. Dai, Investigation on a rotating FGPM circular disk under a coupled hygrothermal field, Appl. Math. Modell., 46 (2017) 28-47.

[12] A. Loghman, M. Abdollahian, A. Jafarzadeh Jazi, A. Ghorbanpour Arani, Semi-analytical solution for electromagneto-thermoelastic creep repose of functionally graded piezoelectric rotating disk, Int. J. Therm. Sci., 65 (2013) 254-266.

[13] A. Ghorbanpour Arani, Z. Khoddami Maraghi, M.R. Mozdianfard, A.R. Shajari, Thermo-piezo-magneto-mechanical stresses analysis of FGPM hollow rotating thin disk, Int. J. Mech. Mater. Des., 6(4) (2010) 341-349.

[14] M. Saadatfar, Time-dependent creep response of magneto-electro-elastic rotating disc in thermal and humid environmental condition, Aust. J. Mech. Eng., 4(1) (2020) 81-90.

[15] M. Bayat, M. Saleem, B.B. Sahari, A.M.S. Hamouda, A. Mahdi, Analysis of functionally graded rotating disks with variable thickness, Mech. Res. Commun., 35(3) (2008) 283-309.

[16] M. Bayat, M. Saleem, B.B. Sahari, A.M.S. Hamouda, A. Mahdi, Mechanical and thermal stresses in a functionally graded rotating disk with variable thickness due to radially symmetry loads, Int. J. Press. Vessels Pip., 86(6) (2009) 357-372.

[17] M. Bayat, B.B. Sahari, M. Saleem, A.M.S. Hamouda, J.N. Reddy, Thermo elastic analysis of functionally graded rotating disks with temperature-dependent material properties: uniform and variable thickness, Int. J. Mech. Mater. Des., 5(3) (2009) 263-279.

[18] A.M. Zenkour, D.S. Mashat, Analytical and numerical solutions for a rotating annular disk of variable thickness, J. Appl. Math., 1(5) (2010) 431-438.

[19] H. Zafarmand, B. Hassani, Analysis of two-dimensional functionally graded rotating thick disks with variable thickness, Acta Mech., 225(2) (2014) 453-464.

[20] A.K. Thawait, L. Sondhi, Sh. Sanyal, Sh. Bhowmick, Elastic analysis of functionally graded variable thickness rotating disk by element based material grading, J. Solid Mech., 9(3) (2017) 650-662.

[21] M.N.M. Allam, R. Tantawy, A.M. Zenkour, Thermoelastic stresses in functionally graded rotating annular disks with variable thickness, J. Theor. Appl. Mech., 56(4) (2018) 1029-1041.

[22] V. Vullo, F. Vivio, Elastic stress analysis of non-linear variable thickness rotating disks subjected to thermal load and having variable density along the radius, Int. J. Solids Struct., 45(20) (2008) 5337-5355.

[23] D. Deepak, V.K. Gupta, A.K. Dham, Creep modeling in functionally graded rotating disc of variable thickness, J. Mech. Sci. Technol., 24(11) (2010) 2221-2232.

[24] A.N. Rybjanets, O.N. Razumovskaja, L.A. Reznitchenko, V.D. Komarov, A.V. Turik, Lead titanate and lead metaniobate porous ferroelectric ceramics, Integr. Ferroelectr., 63(1) (2004) 197-200.

[25] A.N. Rybyanets, Porous piezoelectric ceramics-a historical overview, Ferroelectr., 419(1) (2011) 90-96.

[26] J.F. Li, K. Takagi, M. Ono, W. Pan, R. Watanabe, A. Almajid, M. Taya, Fabrication and evaluation of porous piezoelectric ceramics and porosity-graded piezoelectric actuators, J. Am. Ceram. Soc., 86(7) (2003) 1094-1098.

[27] C.R. Bowen, A. Perry, A.C.F. Lewis, H. Kara, Processing and properties of porous piezoelectric materials with high hydrostatic figures of merit, J. Eur. Ceram. Soc., 24(2) (2004) 541-545.

[28] T.G. Zielinski, Fundamentals of multiphysics modelling of piezo-poro-elastic structures, Arch. Mech., 62(5) (2010) 343-378.

[29] M. Jabbari, M. Meshkini, M.R. Eslami, Non-axisymmetric mechanical and thermal stresses in FGPPM hollow cylinder, J. Pressure Vessel Technol., 134(6) (2012) 061212.

[30] M. Jabbari, M. Meshkini, M.R. Eslami, Mechanical and thermal stresses in FGPPM hollow cylinder due to radially symmetric loads, J. Pressure Vessel Technol., 138(1) (2016) 011207.

[31] M. Meshkini, K. Firoozbakhsh, M. Jabbari, A. SelkGhafari, Asymmetric mechanical and thermal stresses in 2D-FGPPMs hollow cylinder, J. Therm. Stresses, 40(4) (2017) 448-469.

[32] T. Dai, H.L. Dai, Investigation of mechanical behavior for a rotating FGM circular disk with a variable angular speed, J. Mech. Sci. Technol., 29(9) (2015) 3779-3787.

[33] T. Dai, H.L. Dai, Thermo-elastic analysis of a functionally graded rotating hollow circular disk with variable thickness and angular speed, Appl. Math. Modell., 40(17-18) (2016) 7689-7707.

[34] Y. Zheng, H. Bahaloo, D. Mousanezhad, E. Mahdi, A. Vaziri, H. Nayeb-Hashemi, Stress analysis in functionally graded rotating disks with non-uniform thickness and variable angular velocity, Int. J. Mech. Sci., 119 (2016) 283-293.

[35] M. Salehian, B. Shahriari, M. Yousefi, Investigating the effect of angular acceleration of the rotating disk having variable thickness and density function on shear stress and tangential displacement, J. Braz. Soc. Mech. Sci. Eng., 41 (2019) 31.

[36] S.H, Chi, Y.L. Chung, Mechanical behavior of functionally graded material plates under transverse load-Part I: Analysis, Int. J. Solids Struct., 43(13) (2006) 3657-3674.

[37] M. Saadatfar, Effect of interlaminar weak bonding and constant magnetic field on the hygrothermal stresses of a FG hybrid cylindrical shell using DQM, J. Stress Anal., 3(1) (2018) 93-110.

[38] R. Ansari, M. Darvizeh, Prediction of dynamic behaviour of FGM shells under arbitrary boundary conditions, Compos. Struct., 85(4) (2008) 284-292.

[39] M. Saadatfar, M. Aghaie-Khafri, On the magneto-thermo-elastic behavior of a functionally graded cylindrical shell with pyroelectric layers featuring interlaminar bonding imperfections rested in an elastic foundation, J. Solid Mech., 7(3) (2015) 344-363.

[40] M. Saadatfar, Stress redistribution analysis of piezomagnetic rotating thick-walled cylinder with temperature and moisture-dependent material properties, J. Appl. Comput. Mech., 6(1) (2020) 90-104.

[41] A. Behravan Rad, M. Shariyat, Three-dimensional magneto-elastic analysis of asymmetric variable thickness porous FGM circular plates with non-uniform tractions and Kerr elastic foundations, Compos. Struct., 125 (2015) 558-574.

[42] M. Saadatfar, M.H. Zarandi, Deformations and stresses of an exponentially graded magneto-electro-elastic non-Uniform thickness annular plate which rotates with variable angular speed, Int. J. Appl. Mech., 12(5) (2020) 2050050.

[43] M.A. Othman, S.Y. Atwa, The effect of magnetic field on 2-D problem of generalized thermoelasticity with energy dissipation. Int. J. Ind. Math., 3(3) (2011) 213-226.

[44] M. Saadatfar, M.H. Zarandi, Effect of angular acceleration on the mechanical behavior of an exponentially graded piezoelectric rotating annular plate with variable thickness, Mech. Based Des. Struct. Mach., (2020), DOI:10.1080/15397734.2020.1751198.

[45] M. Saadatfar, M.H. Zarandi, M. Babaelahi, Effects of porosity, profile of thickness, and angular acceleration on the magneto-electro-elastic behavior of a porous FGMEE rotating disc placed in a constant magnetic field, Proceedings of the institution of mechanical engineers, J. Mech. Eng. Sci., (2020), DOI:10.1177/0954406220938409.

[46] J.D. Hoffman, Numerical Methods for Engineers and Scientists, CRC Press, 2nd Edition, (2001).

[47] A. Ghorbanpour Arani, H. Khazaali, M. Rahnama, M. Dadkhah, Inhomogeneity material effect on electromechanical stresses, displacement and electric potential in FGM piezoelectric hollow rotating disk, J. Solid Mech., 2(2) (2010) 144-155.

[48] H.L. Dai, Y.M. Fu, J.H. Yang, Electromagnetoelastic behaviors of functionally graded piezoelectric solid cylinder and sphere, Acta Mech. Sin., 23 (2007) 55-63.

[49] H.L. Dai, H.J. Jiang, Analytical study for electromagnetothermoelastic behavior of a functionally graded piezoelectric solid cylinder, Mech. Adv. Mater. Struct., 20(10) (2013) 811-818.